# Dyslipidemia at the crossroad of the skin barrier and the arterial wall

Martins Cardoso, R.

## Chapter 3

# Hyperalphalipoproteinemic scavenger receptor BI knockout mice exhibit a disrupted epidermal lipid barrier

*Biochimica et Biophysica Acta Molecular and Cell Biology of Lipids 1865(3): 158592 (2020).*

Renata Martins Cardoso[1], Eline Creemers[1], Samira Absalah[1], Gert S. Gooris[1], Menno Hoekstra[1], Joke A. Bouwstra[1*], Miranda Van Eck[1*]

[1]Division of BioTherapeutics, Leiden Academic Centre for Drug Research, Leiden University, Leiden, The Netherlands

*Both authors contributed equally

**ABSTRACT**

Scavenger receptor class B type I (SR-BI) mediates the selective uptake of cholesteryl esters (CE) from high-density lipoproteins (HDL). An impaired SR-BI function leads to hyperalphalipoproteinemia with elevated levels of cholesterol transported in the HDL fraction of the plasma. Accumulation of cholesterol in apolipoprotein B (apoB)-containing lipoproteins has been shown to alter skin lipid composition and barrier function in mice. To investigate whether these hypercholesterolemic effects on the skin also occur in hyperalphalipoproteinemia, we compared skins of wild-type and SR-BI knockout (*SR-BI*$^{-/-}$) mice. SR-BI deficiency did not affect the epidermal cholesterol content and induced only minor changes in the ceramide subclasses. The epidermal free fatty acid (FFA) pool was, however, enriched in short and unsaturated chains. Plasma CE levels strongly correlated with epidermal FFA C18:1 content. The increase in epidermal FFA coincided with downregulation of cholesterol and FFA synthesis genes, suggesting a compensatory response to increased flux of plasma cholesterol and FFAs into the skin. Importantly, the *SR-BI*$^{-/-}$ epidermal lipid barrier showed increased permeability to ethyl-paraminobenzoic acid, indicating an impairment of the barrier function. In conclusion, increased HDL-cholesterol levels in *SR-BI*$^{-/-}$ can alter the epidermal lipid composition and lipid barrier function similarly as observed in hypercholesterolemia due to elevated levels of apoB-containing lipoproteins.

***Keywords:*** *High-density lipoprotein, hypercholesterolemia, hyperlipidemia, cholesteryl esters, epidermis, skin lipid metabolism, free fatty acids*

## 1. INTRODUCTION

Lipids are important components of the epidermal stratum corneum (SC), where they form a well-structured lipid matrix that functions as a protective barrier preventing dehydration and the penetration of pathogens and dangerous agents[1]. Cholesterol, ceramides (CERs), and free fatty acids (FFAs) are the main lipid classes present in the SC and are primarily synthesized by differentiating keratinocytes in the epidermis[2]. At the final stage of keratinocyte differentiation, these lipids are extruded into the intercellular space at the interface of the stratum granulosum and the SC and processed to form the SC lipid matrix[3].

Lipids of extracutaneous origin (*e.g.* plasma lipids) may also contribute to the formation of the matrix of SC lipids[4–7]. In plasma, lipids are primarily transported in the core of 4 classes of lipoproteins; chylomicrons, very-low-density lipoproteins (VLDL), and low-density lipoproteins (LDL), and high-density lipoproteins (HDL). Expression of the low-density lipoprotein receptor (LDLR), the apolipoprotein (apo) B/E receptor, in the liver is essential for maintaining normal plasma lipid levels transported by apoB-containing lipoproteins (chylomicrons, VLDL, LDL) and, hence, mutations in the LDLR leads to hyperlipidemia[8–10]. Recent work from our group showed that severe hypercholesterolemia associated with accumulation of apoB-containing lipoproteins can alter the composition of the epidermal lipids and the skin barrier function in mice[11]. Currently, it remains unknown whether the observed effects are specific for apo B-containing lipoproteins.

HDL represents a second important group of lipoprotein particles involved in the transport of cholesterol throughout the body, especially mediating reverse cholesterol transport. HDL particles interact with the ATP-binding cassette transporters ABCA1 and ABCG1[12] to promote cellular efflux of excess cholesterol, which is subsequently stored as cholesteryl esters (CE) in the core of these lipoproteins after esterification by the enzyme lecithin: cholesterol acyl transferase (LCAT)[13]. CE from mature HDL particles can be delivered via the scavenger receptor class B type I (SR-BI) to steroidogenic tissues for hormone production or to the liver to be redistributed to the body or excreted via the bile, the last step in the reverse cholesterol transport process[14,15].

SR-BI is a transmembrane glycoprotein that interacts with HDL and various native and modified lipoproteins (*e.g.* β-VLDL, oxidized LDL)[16,17]. In addition to its high expression in the liver and in steroidogenic tissues, SR-BI, like the LDLR, is also expressed in the epidermis; especially in keratinocytes in the basal epidermal layer close to the vascular bed in the dermis[4,7,18,19]. The expression of this receptor decreases towards the skin

surface but is increased in case of barrier disruption or inhibition of local synthesis by statins[4,7]. In contrast with apoB-containing lipoproteins, which deliver their lipid content via receptor mediated uptake, smaller HDL particles can more efficiently move through tissues (plasma to interstitial fluid) and get into the skin[20]. In fact, the skin is one of the largest body reservoirs of HDL[21].

In both mice and humans, impaired reverse cholesterol transport due to deficiency or polymorphisms in the gene encoding for SR-BI results in hyperalphalipoproteinemia marked by an accumulation of larger and abnormal HDL particles and increases HDL-cholesterol in the circulation[10,22,23]. Among others, HDL-driven hyperalphalipoproteinemia, a special form of hypercholesterolemia, has been related to altered platelet function[24,25] and reduced steroidogenesis[23,26,27].

In this study, we aimed to investigate whether hyperalphalipoproteinemia and the associated increase in HDL-cholesterol would affect the skin lipid barrier. For this purpose, we compared the skin of *SR-BI* knockout (*SR-BI*$^{-/-}$) mice, a model for hyperalphalipoproteinemia, to the skin of wild-type (WT) control mice of similar age and genetic background. Hereto, we assessed the skin morphology, the composition and organization of the epidermal lipids, and the lipid barrier function. The experimental mice were fed a low fat/low cholesterol diet as we aimed to specifically analyze the effects of HDL-driven hyperalphalipoproteinemia in absence of high fat/high cholesterol diet-induced increases in apoB-containing lipoproteins.

## 2. MATERIALS AND METHODS

### 2.1 Chemicals

Rodent chow diet low in fat and cholesterol (Rat and Mouse No.3 breeding diet) was purchased from Special Diets Services (United Kingdom). We obtained ketamine and atropine from AUV Veterinary Services (Cuijk, The Netherlands) and xylazine from ASTFarma (Oudewater, The Netherlands). Sodium phosphate dibasic ($Na_2HPO_4$), hematoxylin, eosin, toluidine blue, trypsin from bovine pancreas, trypsin inhibitor, cholesterol, FFA with carbon chains ranging from 16 to 30 carbon atoms (FFA C16-30), deuterated FFA C18, deuterated FFA C24, chloroform, acetic acid, deuterated water, natrium bromide (NaBr), ethyl-para-aminobenzoic acid (E-PABA), trifluoroacetic acid, synthetic CER N(24)dS(18), CER N(24)S(18), CER N(24)P(18), and CER A(24) S(18) were obtained from Sigma-Aldrich (Zwijndrecht, The Netherlands). Synthetic CER E(18:2)O(30)S(18) and CER[N(C24deuterated)S(C18protonated)] were kindly provided by Evonik Industries (Essen, Germany). Sodium chloride (NaCl) and Kaiser's

glycerol gelatin were purchased from Boom (Meppel, The Netherlands). Heptane was purchased from ChemLab (Zedelgem, Belgium). Potassium dihydrogen phosphate ($KH_2PO_4$), potassium chloride (KCl) and Entellan® were purchased from Merck (Darmstadt, Germany). Methanol, ethanol, isopropanol and acetonitrile were purchased from Biosolve (Valkenswaard, The Netherlands). All solvents used were analytical grade.

### 2.2 Animals



Female C57Bl/6 WT mice were obtained from The Jackson laboratory and bred at the Gorlaeus laboratories. Female homozygous *SR-BI*$^{-/-}$ mice were kindly provided by Monty Krieger and cross-bred at the Gorlaeus laboratories to a C57Bl/6 background. The experimental WT group consisted of the same mice as reported previously[11]. The mice were kept under standard laboratory conditions at 20°C and with light cycle of 12 hours light/12 hours dark. The mice received water and standard low-fat chow diet ad libitum (Rat and Mouse No. 3 breeding diet). At 16-18 weeks of age the mice were anesthetized with xylazine (70 mg/kg body weight), atropine (1.8 mg/kg body weight), and ketamine (350 mg/kg body weight) followed by retro-orbital bleeding and perfusion with phosphate buffered saline (PBS, 8.13 g/L NaCl, 2.87 g/L $Na_2HPO_4$, 0.2 g/L $KH_2PO_4$, 0.19 g/L KCl in milliQ water pH 7.4) at room temperature. Blood was collected in EDTA-containing tubes. The dorsal skin of the mice was shaved and the skin was processed further for morphological stainings, lipid and gene expression analysis. All experiments were in agreement with National guidelines and approved by the Animal Experiments Ethics Committee of Leiden University.

### 2.3 Plasma lipid analysis

Non-fasted plasma levels of free cholesterol (FC), cholesteryl esters (CE) and triglycerides were measured by enzymatic colorimetric assays performed as described previously (Roche Diagnostics, Almere, Netherlands)[28].

### 2.4 Skin morphology staining

4-5 µm paraffin sections of skin were stained with hematoxylin and eosin or with toluidine blue as described previously[11]. Stained sections were mounted in Entellan® and imaged with a Zeiss Axioplan 2 light microscope (Zeiss, Best, The Netherlands). The presence of cholesterol crystals was verified using a BH-2 polarized microscope (Olympus, Leiderdorp, The Netherlands).

### 2.5 Liquid chromatography-mass spectrometry (LC/MS)

Skin samples without the hypodermis were stretched on a paper filter soaked in 0.3 % w/v trypsin solution in PBS (pH 7.4) overnight at low temperature (4°C). The next day, the skin was incubated at 37°C (1 hour) for trypsin activation and subsequently the epidermis was isolated. Afterwards, the trypsin in the samples was neutralized by washing the samples in 0.1% w/v trypsin inhibitor in PBS (pH 7.4) and in demi-water. After air-drying, the epidermis was stored under argon atmosphere for further SC lipid extraction followed by LC/MS analysis, and Fourier transform infrared spectroscopy (FTIR). Epidermal lipids were extracted as described by Boiten *et. al.* (2016) and the extracts were stored in chloroform:methanol (2:1; v/v) at 4°C under argon atmosphere for LC/MS-based cholesterol, CER and FFA analysis[29].

*Cholesterol and CER analysis*

Epidermal cholesterol and CER analysis by LC/MS was performed as described previously[11]. In short, epidermal lipid extracts (dried at 40°C under a gentle flow of nitrogen) were reconstituted to a lipid concentration of 0.3 mg/ml in heptane:chloroform:methanol (95:2.5:2.5; v/v/v). Deuterated CER[N(C24deuterated) S(C18protonated)] was added to all samples as internal standard. Reconstituted epidermal lipid extracts (5 µl) were injected using an Acquity UPLC H-class system (Waters, Milford, MA, USA). Separation was achieved on a normal phase column (PVA-Sil column: 5 µm particle size, 100x2.1 mm i.d., YMC, Kyoto, Japan) with an eluent flow rate of 0.8 ml/min (Supplementary Table S1). The UPLC system was connected to a XEVO TQ-S mass spectrometer (Waters, Milford, MA, USA) with an atmospheric pressure chemical ionization (APCI) chamber. Samples were measured with positive ion detection mode for full scans (350-1200 amu) and the area under the curve (AUC) was determined using Waters MassLynx 4.1 software and corrected for the internal standard. Cholesterol data was plotted as absolute amount of cholesterol per epidermis weight (µg/mg) based on a calibration curve of cholesterol. CER composition data was plotted as relative percentage of each ceramide subclass based on AUC values corrected for internal standard. This method can underestimate the level of [EO] subclasses. CERs nomenclature as described by Motta *et al.* (1993) depicting the acyl chains (non-hydroxy fatty acid [N]; α-hydroxy fatty acid [A] or esterified ω-hydroxy fatty acid [EO]) and the sphingoid base (dihydrosphingosine, [dS]; sphingosine [S] or phytosphingosine [P])[30].

*FFA analysis*

Epidermal FFA analysis by LC/MS was performed using the same UPLC/MS system described above. Epidermal lipid extracts (dried at 40ºC under a gentle flow of nitrogen) were reconstituted in isopropanol to a lipid concentration of 0.75 mg/ml. Next, internal standards deuterated FFA C18 and deuterated FFA C24 were added to the samples. Reconstituted lipid extracts (2 µl) were injected in the UPLC system into a Purospher Star LiChroCART reverse phase column (3 µm particle size, 55x2 mm i.d., Merck, Darmstadt, Germany) with an eluent flow rate of 0.5 ml/min (Supplementary Table S2). The XEVO TQ-S mass spectrometer coupled to the APCI (probe temperature: 425°C, discharge current 3 µA.) was set to negative ion mode and the detector measured full scans (200-550 amu). Data was analyzed using Waters MassLynx 4.1 software to determine the AUC. The AUC was corrected for the internal standard FFA C24 and calculated to absolute amounts based on calibration curves of FFA C16-C30. FFA composition was plotted in absolute amounts and as relative percentage to the total amount FFA detected (%w/w). FFA C16:0 and C18:0 were not plotted as they were present in the solvent used for lipid extraction due to manufacturer's contamination with these FAs. Unsaturated FFA C16-C18, important components of sebum lipids, were plotted separately[31,32].

**2.6 CER fragmentation by (LC/)MS/MS**

Murine CERs present in the epidermal lipid extract (in chloroform-methanol 2:1) were separated using the UPLC-H class system described above for CER analysis while maintaining a continuous solvent flow of 98% heptane and 2% heptane:isopropanol:ethanol (50:25:25; v/v/v) at 0.8 ml/min. Fragmentation spectra (MS/MS) of murine epidermal CERs were obtained using the XEVO TQ-S mass spectrometer. The collision energy for MS/MS was set to 30 eV. All other parameters of the XEVO TQ-S mass spectrometer were identical to the setup described for CER analysis. Parent ions with masses of 647, 653 and 663 amu were fragmented and identification of the fragments was performed using Waters MassLynx 4.1.

**2.7 q-PCR**

Total RNA was isolated from skin samples after removal of the hypodermis using the guanidinium thiocyanate method[33]. 1 µg of RNA was used to synthesize cDNA using M-MuLV reverse transcriptase. SYBR Green Technology was used for the quantitative gene expression analysis with a 7500 Fast real-time PCR system (Applied Biosystems, Foster City, CA, USA). Gene expression was normalized by the expression of the

housekeeping genes ribosomal protein, large, P0 (*RPL0*), cytochrome c-1 (*CYC1*) and ribosomal protein S20 (*RPS20*). Relative gene expression was determined as the difference between the average threshold cycle (Ct) of the housekeeping genes and the Ct of the target gene followed by raising this difference to the power of 2. The expression of target genes in the *SR-BI*$^{-/-}$ skin were plotted as relative fold change compared to the WT controls. Forward and reverse primer sequences of the housekeeping genes and genes of interest are available in Supplementary Table S3.

### 2.8 Fourier transformed infrared spectroscopy

Epidermis was hydrated for 24 hours over 27% sodium bromide in deuterated water and placed between two silver bromide windows for Fourier transform infrared spectroscopy (FTIR) measurements (Varian 670-IR spectrometer, Agilent Technologies, Inc., Santa Clara, CA). The spectrometer was equipped with a broad-band mercury cadmium telluride detector. FTIR spectra (600-4000 $cm^{-1}$) were collected within a temperature range from 0-90°C rising at a rate of 0.5°C/min. Deconvolution of the spectra (half width of 4 $cm^{-1}$; enhancement factor of 1.7) was processed with Resolutions Pro 4.1 (Varian Inc.) software. Lateral organization of the SC lipids was monitored by $CH_2$ rocking vibrations (710-750 $cm^{-1}$). The ratio between the peak area at 730 $cm^{-1}$ and the area peak at 719 $cm^{-1}$ was used to assess changes in the fraction of lipids adopting the orthorhombic phase at 32°C (skin temperature). This area ratio was calculated by curve fitting these two main peaks in the region of $CH_2$ rocking vibrations of the FTIR spectra using a Lorentzian peak function. The transition temperature between the orthorhombic and hexagonal phases was determined by the disappearance of the vibration at the 730 $cm^{-1}$.

### 2.9 Transepidermial water loss (TEWL)

Transepidermal water loss (TEWL) was measured in the skin of WT and *SR-BI*$^{-/-}$ mice to assess the barrier the skin barrier function. For TEWL measurements the mice were anesthetized as described on section 2.2 and their dorsal skin was shaved. The closed-chamber of the evaporimeter (Aqua Flux AF200, Biox Systems Ltd, London, UK) was placed in upright position on their dorsal skin perpendicular to the skin surface. Transepidermal water loss was measured for 120 seconds. The temperature in the room (22°C) and the humidity (50.1%) were controlled during the measurements.

### 2.10 Murine lipid model membranes (mLMM)

Murine lipid model membranes (mLMM) mimicking either the lipid composition of

the epidermis of WT or *SR-BI*$^{-/-}$ mice were prepared based on the lipid composition determined by LC/MS in this study. All mLMM were prepared with a CER mixture containing CER N(24)dS(18), CER N(24)S(18), CER N(24)P(18), CER A(24)S(18), CER E(18:2)O(30)S(18) in a molar ratio of 40.5:36:5:14.5:4, respectively. The FFAs were composed of FFA C16:0, C18:0, C20:0, C20:1, C22:0, C22:1, C24:0, C26:0 in a molar ratio representative of either WT or *SR-BI*$^{-/-}$ mice SC FFA composition (Table 1). Briefly, for mLMM preparation all lipids were collected in a glass vial, dried under a gentle nitrogen flow and reconstituted in hexane:ethanol (2:1; v/v) to a lipid concentration of 5 mg/ml. The lipid mixtures were sprayed under a gentle nitrogen flow onto a polycarbonate membrane (0.05 µm pore size, 25 mm i.d., Whatmann, Kent, UK) using a 100 µl Hamilton syringe, Bonaduz, Switzerland). Spraying (5 µl/min) was performed by a Camag Linomat IV with an extended y-axis arm (Muttenz, Switzerland) to form a homogeneous square of 10 x 10 mm. Sprayed mLMMs were equilibrated at 85°C for 10 minutes, cooled down to room temperature for storage under argon atmosphere until their use in the permeability studies.

**Table 1. FFA composition of mLMM prepared for permeability studies.**

| FFA Standard | FFA WT (%Molar ratio) | FFA *SR-BI*$^{-/-}$ (%Molar ratio) |
|---|---|---|
| C16:0 | 3.5 | 4.0 |
| C18:0 | 1.5 | 1.0 |
| C20:0 | 2.0 | 5.5 |
| C20:1 | 10.0 | 20 |
| C22:0 | 4.5 | 5.5 |
| C22:1 | 3.5 | 4.0 |
| C24:0 | 30.0 | 29.0 |
| C26:0 | 45.0 | 31.0 |

### 2.11 Lamellar and lateral organization of mLMM

X-ray diffraction studies (station BM26B, European Synchrotron Radiation facility, Grenoble, France) were used to determine both lamellar and lateral organization of the mLMM. After hydration (24 hours, 27% sodium bromide in demiwater) the mLMM were mounted into a sample holder (parallel to X-ray beam; X-ray wavelength of 0.1034 nm, sample-to-detector distance of 1980 mm) with the temperature controlled at 25°C.

Small angle X-ray diffraction data were collected on a Pilatus 1M detector (1043 × 981 pixels at 172 x 172 µm spatial resolution) calibrated using silver behenate (d = 5.838 nm). Wide angle X-ray diffraction data were collected on a Pilatus 300K (1475 × 195 pixels at 172 x 172 µm spatial resolution, sample-to-detector distance of 3110 mm) calibrated using the high density polyethylene (HDPE, d = 0.416 nm and 0.378 nm). The scattering intensity I (in arbitrary units) of the static diffraction patterns (collected for 60 seconds at two positions) was calculated as a function of the scattering vector q (in reciprocal nm). Vector $q$ was determined as shown in Equation 1 with $\theta$ representing the scattering angle and $\lambda$ the wavelength. Diffraction rings were integrated over an angle of 40°. The periodicity (d-spacing) of the lamellar phase was calculated as shown in Equation 2 using the the positions of a sequence of equidistant peaks ($q_n$) with n representing the order number of the diffraction peak.

$$\textit{Equation 1: } q = (4\pi \sin\theta)/\lambda$$

$$\textit{Equation 2: } d = 2n\pi / q_n$$

### 2.12 Permeability studies with mLMM

Ethyl-para-aminobenzoic (E-PABA) was used as a model drug to assess the functionality of the mLMMs as a lipid barrier. mLMMs were mounted into Permegear inline diffusion cells (0.282 $cm^2$ diffusion area, Bethlehem PA, USA). The donor phase was composed of saturated E-PABA solution (0.65 mg/ml, pH 5.0), while the acceptor phase was comprised of PBS (pH 7.4, stirring at 50 rpm, flow rate 2-2.5 ml/min). For 10 hours the acceptor PBS phase was collected in 1 hour fractions (Isco Retriever IV; Teledyne Isco, Lincoln NE, USA) and the E-PABA content was determined by UPLC-UV (Waters, Etten-Leur, The Netherlands) with acetonitrile with 0.1% trifluoroacetic acid:milliQ (40:60; v/v) as mobile phase (flow rate of 0.5 ml/min). Separation occurred in a reversed phase C18 column (Alltima, C-18, 1.7 µm i.d., 2.1 x 50 mm, Waters, Ireland) followed by UV detection (excitation wavelength = 286 nm). A calibration curve of E-PABA in methanol was included in the UPLC-UV analysis for E-PABA quantification. Data was analyzed with the software TargetLynx. Average steady-state fluxes were calculated as the average flux measured from 3.5 to 10.5 hours.

### 2.13 Statistical analysis

Statistical analysis was performed using GraphPad Prism 7 (GraphPad Software Inc., CA, USA). Data are presented as means±SD. Significant differences between groups were determined by two-tailed unpaired students t-Test. Correlations between parameters were determined using a Pearson's correlation coefficient analysis and linear regression.

*P* values below 0.05 were considered significant.

## 3. RESULTS

### 3.1 Plasma lipid profile and skin morphology

The plasma lipid profile of non-fasted female WT and *SR-BI*$^{-/-}$ mice was determined by enzymatic colorimetric assays (Figure 1a). On a low-fat chow diet SR-BI deficiency in mice generally results in increased plasma cholesterol levels driven by an increase in HDL-cholesterol[10]. In agreement, *SR-BI*$^{-/-}$ mice in this study displayed a hypercholesterolemic plasma lipid profile marked by a significant increase in FC (1.20±0.25 µg/µl plasma; $p<0.0001$) and CE (1.37±0.3 µg/µl plasma; $p<0.0001$) levels compared to normolipidemic WT controls (FC 0.36±0.05 µg/µl plasma; CE 0.85±0.08 µg/µl plasma). The levels of plasma triglycerides in *SR-BI*$^{-/-}$ mice did not differ from those of WT mice.

Next, we evaluated the morphology of the skin of the mice by hematoxylin and eosin or toluidine blue stainings of paraffin sections (Figure 1b). Similar to WT controls, the skin of *SR-BI*$^{-/-}$ mice showed a thin SC, no epidermal hyperproliferation, and no evidence of inflammation as illustrated by the absence of immune cell infiltrates. The morphology of the dermis was also not altered. Polarized microscopy did not reveal the presence of cholesterol crystals in the sections (data now shown).

### 3.2 Epidermal lipid composition

The three main barrier lipid classes (cholesterol, CERs and FFAs) in the epidermis of *SR-BI*$^{-/-}$ mice were analyzed by LC/MS and compared to WT controls. The amount of cholesterol in the *SR-BI*$^{-/-}$ epidermis (27.4±5.3 µg/mg epidermis) was comparable to the WT control (28.7±3.1 µg/mg epidermis) (Figure. 2a). In both WT and *SR-BI*$^{-/-}$ epidermis seven subclasses of CER were detected: CER NdS, CER NS, CER NP, CER AdS, CER AS, CER EOdS, and CER EOS (Figure 2b-c). In the epidermis of *SR-BI*$^{-/-}$ mice, the abundance of CER AS (10.8±0.6%) was lower than in the WT control (13.5±1.1%; $p<0.01$). In contrast, the abundance of CER EOS was increased in the *SR-BI*$^{-/-}$ epidermis (6.9±1.0%) compared to the WT epidermis (4.6±0.7%; $p<0.01$). CER NP and CER AdS were not fully separated in the ion map; thus, these CER subclasses were grouped together, accounting for nearly 5% of the total CER content in the epidermis of both types of mice. Interestingly, a slight increase in the average CER chain length was observed in the *SR-BI*$^{-/-}$ epidermis for the non-ω-esterified (CER[nonEO]) (42.3±0.1 carbon atoms) and for the ω-esterified (CER[EO]) (68.2±0.1 carbon atoms) CER subclasses compared to

the WT epidermis (42.0±0.1 and 67.5±0.1 carbon atoms, respectively; $p<0.005$) (Figure 2d-e and Supplementary Figure S1).

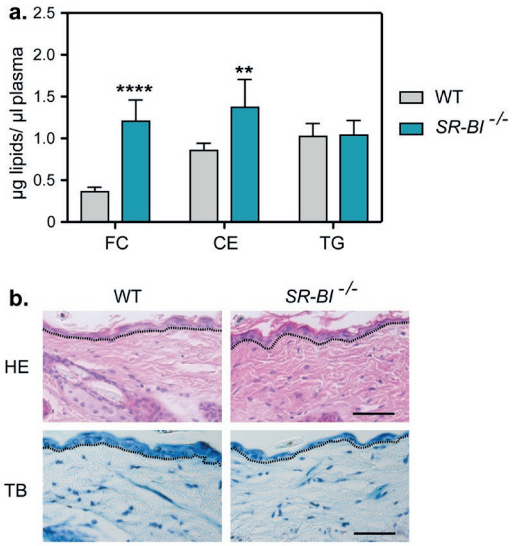


**Figure 1. Non-fasted plasma lipids levels and skin morphology of WT and *SR-BI*$^{-/-}$ mice.** a. Plasma levels of free cholesterol (FC), cholesteryl esters (CE), and triglycerides (TG) (n=5-6 animals/group). b. Representative paraffin sections of skin stained with hematoxylin and eosin (HE) or toluidine blue (TB). The interface between epidermis and dermis is marked by a black dashed line. Scale bar: 50 µm. Data shown as mean±SD. Significant differences between groups were determined by two-tailed unpaired student's t-Test. **$p<0.01$ and ****$p<0.0001$.

The CER chain length distribution revealed unusual abundance of CERs containing odd-numbered carbon chains (Figure 2d-e). In particular, CER[nonEO] containing 43 carbons atoms and CER[EO] containing 67 carbon atoms were abundantly present in both WT and *SR-BI*$^{-/-}$ epidermis. Further investigation with MS/MS fragmentation of CER NS C42 and CER NS C43, two CERs abundantly present in the epidermis, showed clear fragments for the fatty acid chain and the sphingosine base of these CERs as previously described[34]. For CER NS C42 with the parent ion $[M+H-H_2O]^+$ (m/z 632.3), fragments related to a fatty acid chain of 24 carbons atoms were detected at m/z 368.3 $[M+H-C_{16}H_{31}OH]^+$. Moreover, highly abundant fragments characteristic of a sphingosine base with 18 carbon atoms were found at m/z 252.3 $[M+H\text{-FA chain-}CH_3OH]^+$, 264.3 $[M+H\text{-FA chain-}H_2O]^+$ and 282.2 $[M+H\text{-FA chain}]^+$. Additionally, $[M+H\text{-FA chain-}H_2O]^+$ fragments, characteristic of sphingosine bases containing 16 and 17 carbon atoms, were detected at lower abundance at m/z

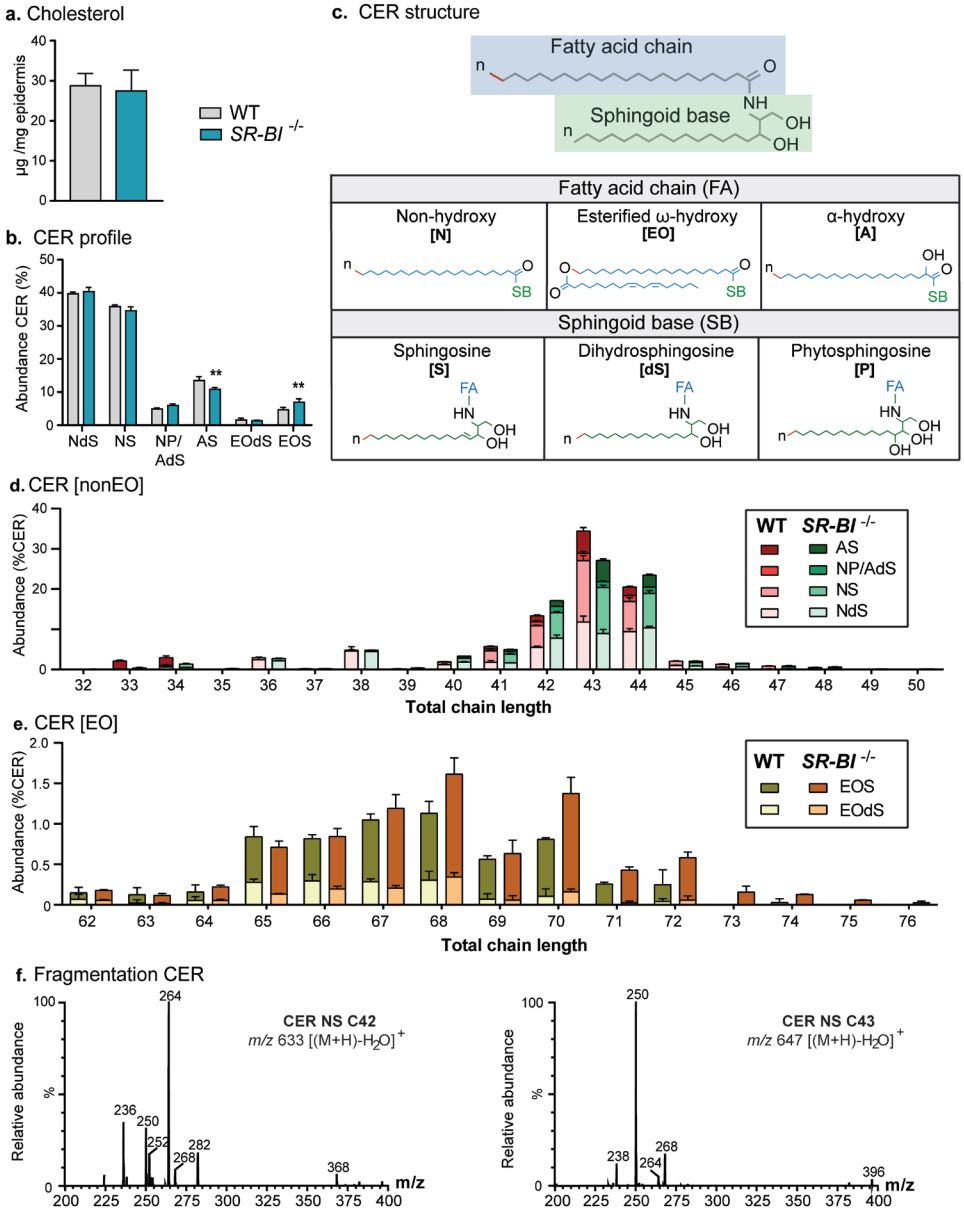


**Figure 2. CER composition in the epidermis of WT and *SR-BI*$^{-/-}$ mice determined by LC/MS analysis.** (a) Schematic representation of the molecular structure of CERs subclasses named as described by Motta *et. al.* (1993); (b) CER profile depicting the detected CER subclasses (NdS, NS, NP, AdS, AS, EOdS, EOS); (c) average total chain length of CERs with non-ω-esterified (CER[nonEO]) and ω-esterified (CER[EO]) fatty acid chains in their acyl chain; (d-e) CER chain length distribution of CER[nonEO] and CER[EO]; (f) MS/MS fragmentation of CER NS C42 and CER NS C43 showing an ion spectra in the range 200-700 m/z. Values are plotted as

mean±SD (n=3 animals/group). Statistical significance was determined by two-tailed unpaired student's t-Test. *$p$<0.05; **$p$<0.01.

236.1 and 250.1, respectively. In contrast, fragmentation of the CER NS C43 parent ion $[(M+H)-H_2O]^+$ at m/z 646.6 showed high abundance of fragments typical of a sphingoid base of 17 carbon atoms at m/z 238.1 $[M+H\text{-FA chain-}CH_3OH]^+$, 250.1 $[M+H\text{-FA chain-}H_2O]^+$, 268.1 $[M+H\text{-FA chain}]^+$. In addition, an abundant fragment of fatty acid with a chain of 26 carbons $[M+H-C_{18}H_{35}OH]^+$ was detected at m/z 396.2.

Epidermal FFA species with carbon chains ranging from 20-30 carbon atoms and abundant monounsaturated species were quantified by LC/MS (Figure 3a-b). Significant differences in the FFA profile between the *SR-BI*$^{-/-}$ mice and WT controls were detected. The epidermis of *SR-BI*$^{-/-}$ mice contained higher levels of FFAs with a chain length from 20 to 30 carbon atoms per mg of epidermis compared to WT controls (3.4±0.5 vs. 6.2±0.1 µg FFA/mg epidermis; $p$<0.01) (Figure 3c and Supplementary Figure S2). In the epidermis of both types of mice FFA C24:0 and FFA C26:0 were the most abundant FFA species. When focusing on the relative values (µg FFA/µg total FFA x 100%), FFA C26:0 represented 44% of the FFA species in the WT epidermis, while FFA C24:0 comprised 25% (Figure 3b). In contrast, in the epidermis of *SR-BI*$^{-/-}$ mice FFA C24 and FFA C26:0 were nearly equally abundant as a result of a strong reduction in the abundance of FFA C26:0 to only 28% ($p$<0.0001). Furthermore, the abundance of monounsaturated FFAs showed a 2-fold ($p$<0.05) increase in the *SR-BI*$^{-/-}$ epidermis (Figure 3d); in particular, FFA C20:1 (16%) was markedly increased compared to the WT controls (7.4%; $p$<0.0001). FFAs with a chain length containing less than 24 carbon atoms accounted for approximately 30% of the FFA species present in the epidermis of *SR-BI*$^{-/-}$ mice, while in WT mice these FFAs comprised 17% of FFAs (Figure 3e). As a result, the mean carbon chain length of the FFAs (including both saturated and unsaturated FFAs) in the *SR-BI*$^{-/-}$ mice was shorter than in the WT counterparts (Figure 3f; $p$<0.01).

### 3.3 Plasma cholesterol esters and skin FFA C18:1 and FFA C20:1 content

Our previous studies showed that the epidermis of hypercholesterolemic apolipoprotein E knockout mice (*APOE*$^{-/-}$) with severely elevated plasma CE levels is significantly enriched in FFA C18:1[11]. Likewise, in the current study *SR-BI*$^{-/-}$ mice with a mild increase in plasma CE exhibited higher levels of epidermal FFA C18:1 (Figure 4a). Therefore, the plasma CE concentration was plotted against the levels of FFA C18:1 in the epidermis of *SR-BI*$^{-/-}$mice (current study) and in the epidermis of *APOE*$^{-/-}$ mice (previously published study)[11]. The plasma CE levels WT and *SR-BI*$^{-/-}$ (moderately elevated CE) and

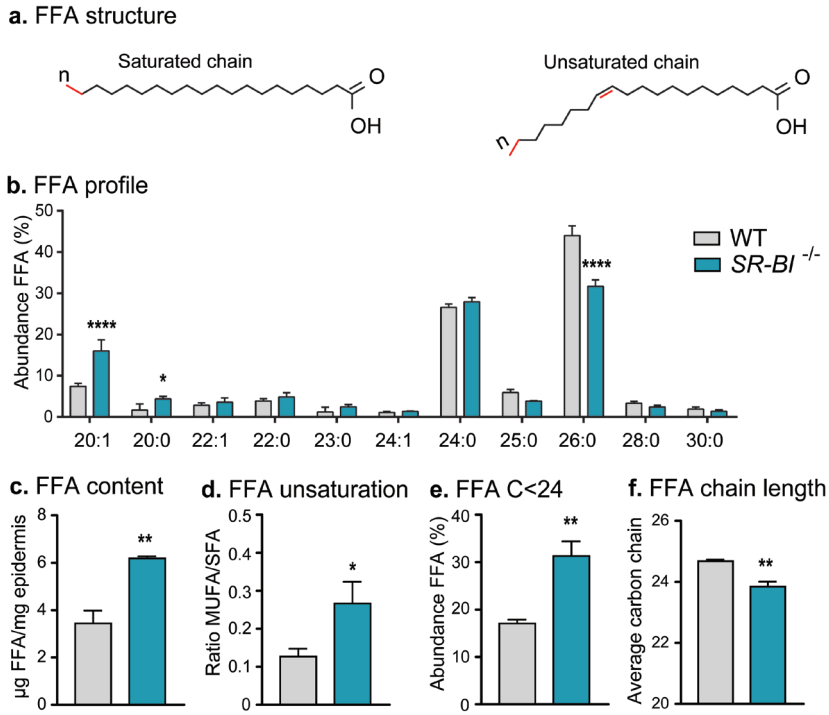


**Figure 3. FFA composition in the epidermis of WT and *SR-BI*$^{-/-}$ mice determined by LC/MS analysis.** (a) Schematic representation of the molecular structure of saturated and monounsaturated FFAs; (b) FFA profile; (c) Total FFA content (C20-C30) per mg of extracted epidermis; (d) FFA unsaturation ratio (MUFA-monounsaturated fatty acid, SFA- saturated fatty acid); (e) Abundance of FFA chains with less than 24 carbons atoms; (f) average FFA chain length. Values are plotted as mean±SD (n=3 animals/group). Statistical significance was determined by two-tailed unpaired student's t-Test. *$p$<0.05; **$p$<0.01; ****$p$<0.0001.

*APOE*$^{-/-}$ (severely elevated CE) showed a strong positive correlation with epidermal FFA C18:1 levels (Pearson's $r$ = 0.9510, $p$<0.0001). In the epidermis FFA C18:1 can be elongated to FA C20:1[35]. Correspondingly, the epidermal levels of FFA C18:1 showed a significant linear correlation with the epidermal levels of FFA C20:1 (Pearson's $r$ = 0.9448, $p$=0.0001; Figure 4c).

### 3.4 Skin gene expression

To gain insight in the effects and underlying causes of differences observed between the barrier lipid profile of WT control and *SR-BI*$^{-/-}$ mice, the expression of genes involved in skin lipid biosynthesis, uptake, efflux and degradation was analyzed by qPCR.

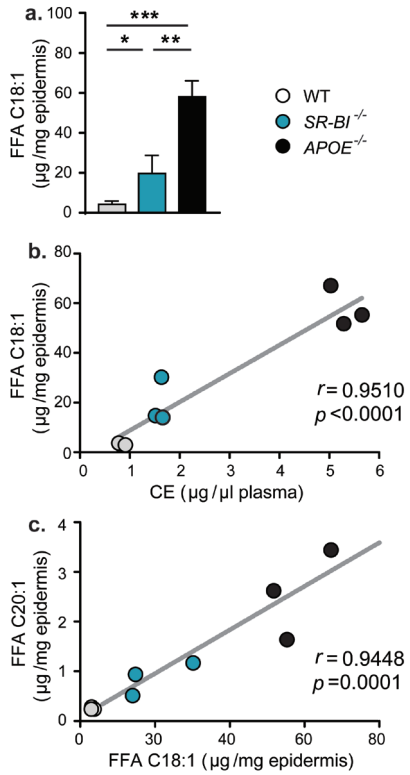


**Figure 4. Correlation between plasma CE concentrations and unsaturated FFAs in the epidermis of WT, *SR-BI*$^{-/-}$ and *APOE*$^{-/-}$ mice.** a. Epidermal levels of FFA C18:1; b. correlation between plasma CE concentration and epidermal FFA C18:1; c. correlation between epidermal FFA C18:1 and FFA C20:1. Plasma CE levels were determined by colorimetric enzymatic assays performed according to manufacturer's instructions. Epidermal FFA C18:1 and FFA C20:1 were determined by LC/MS analysis. Data regarding plasma CE, epidermal FFA C18:1 and FFA C20:1 levels of *APOE*$^{-/-}$ mice were obtained from a previous publication[11]. Data shown as mean±SD. Significant differences among groups were determined using One-way ANOVA with Holm-Šídák post-hoc test (*$p$<0.05; **$p$<0.01; ***$p$<0.001). Correlation between parameters was analyzed using Pearson's correlation analysis (r and p values) and linear regression (black line).

In the skin of *SR-BI*$^{-/-}$ mice the expressions of *HMGCS1* (cholesterol synthesis) and *LDLR* (lipoprotein uptake) were strongly downregulated (1.7-fold and 2.4-fold reduction, respectively) as compared to WT controls ($p$<0.05) (Figure 5a). For the CER metabolic pathways, comparable mRNA levels of *CERS3* (sphingolipid-based ceramice synthesis) were observed in the skin of WT and *SR-BI*$^{-/-}$ mice, while *GBA* (glucosylceramide metabolism) expression was reduced in the *SR-BI*$^{-/-}$ skin (1.6-

fold, $p$<0.05; Figure 5a). Regarding FFAs in the skin (Figure 5b), significantly lower mRNA levels of *ACACA* (2.1-fold; $p$<0.01) and *FAS* (1.7-fold; $p$<0.05), key enzymes in fatty acid synthesis, were detected in the *SR-BI*$^{-/-}$ skin, which was associated with a parallel reduction in the expression of *ELOVL1* (fatty acid chain elongation) (2.6-fold, $p$<0.05). *SCD1* expression (production of monounsaturated FFAs) in *SR-BI*$^{-/-}$ skin was equivalent to that observed in the WT controls. No significant differences were observed in the expression of genes encoding for ATP-binding cassette transporters, ceramide degradation enzymes and other elongases (Supplementary Figure S3). Despite the recently described *in vitro* effect of *SR-BI* knockdown on peroxisome proliferator-activated receptors[36], no differences on mRNA levels were noted for these genes in our experimental setting. In addition, in agreement with the morphological stainings, no significant differences were observed in the expression of genes related to keratinocyte proliferation and differentiation (*IVL, FLG, K10*) (data not shown).

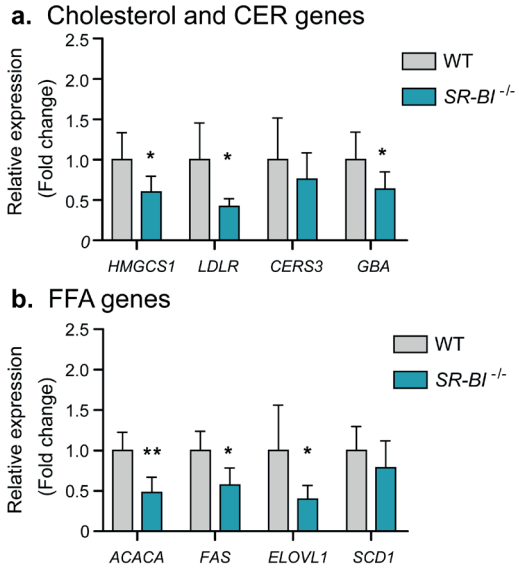


**Figure 5. Effect of *SR-BI* deficiency on the expression of genes involved in lipid uptake and lipid synthesis in the skin.** Relative mRNA expression levels of genes involved in (a) cholesterol and CER synthesis and (b) FFA synthesis. Genes and their respective encoded proteins/receptors: HMGCS1 - 3-hydroxy-3-methylglutaryl-Coenzyme A synthase 1; LDLR - low density lipoprotein receptor; CERS3 - ceramide synthase 3; GBA – glucocerebrosidase; ACACA - acetyl-Coenzyme A carboxylase alpha; FAS – fatty acid synthase; ELOVL1 - elongase of very long chain fatty acids 1; SCD1 - stearoyl-Coenzyme A desaturase 1. Values are plotted as mean±SD representing the fold change expression compared to the WT control (n=5-6 animals/group). Statistical significance was determined by two-tailed unpaired student's t-Test. *$p$<0.05; **$p$<0.01.

### 3.5 Lateral lipid organization

The epidermal lipid composition influences the lateral packing of these lipids, one of the determining parameters for the functionality of the skin barrier. The lateral lipid organization of the *SR-BI*$^{-/-}$ epidermis was analyzed by FTIR and compared to WT controls. In the spectrum region of the $CH_2$ rocking vibrations (710-740 $cm^{-1}$) a doublet at 710 $cm^{-1}$ and at 730 $cm^{-1}$, indicative of a dense orthorhombic lateral lipid packing, was present in both WT and *SR-BI*$^{-/-}$ epidermis (Figure 6a). At 32°C (skin surface temperature) the fraction of lipids adopting an orthorhombic organization was comparable between the groups: a similar ratio between the peak area at 730 $cm^{-1}$ and at 719 $cm^{-1}$ was observed (Figure 6b). The orthorhombic to hexagonal transition temperature was determined by the disappearance of the peak at 730 $cm^{-1}$ as a function of temperature. This transition temperature varied between 38°C and 44°C in both groups (Figure 6c).

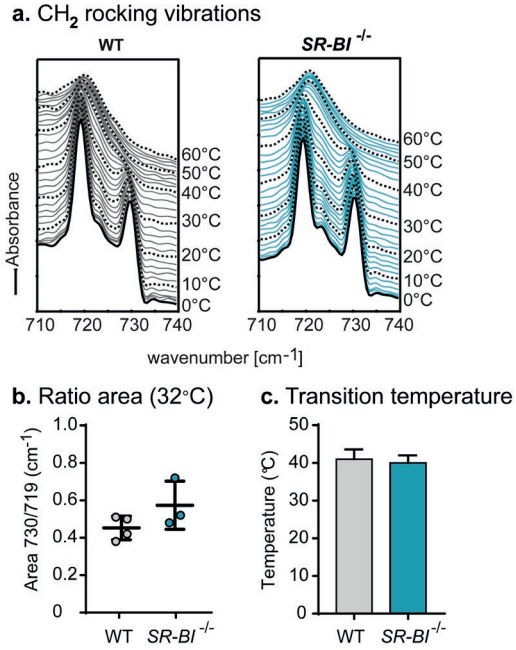


**Figure 6. Lateral lipid organization in WT and *SR-BI*$^{-/-}$ epidermis. Lateral lipid organization was assessed by FTIR.** (a) $CH_2$ rocking vibrations (710-740 $cm^{-1}$) were plotted as a function of temperature (0-60°C) to determine the lateral lipid packing; (b) area ratio between the peak at 730 $cm^{-1}$ and the peak at 719 $cm^{-1}$ at 32°C (skin surface temperature); (c) average transition temperature from orthorhombic and hexagonal phases. Values are plotted as mean±SD (n=3-4 animals/group). No statistical significant differences were observed by two-tailed unpaired student's t-Test.

### 3.6 Permeability studies using mLMMs

In non-nude mice, the isolation of SC or viable epidermis is hampered by the large number of hair follicles present in their skin. In addition, hair follicles may offer another route of permeation to compounds, which in turn compromises the analysis of the effects of the altered lipid barrier function[37,38]. Nonetheless, the inside-outside skin barrier function was analyzed *in vivo* by transepidermal water loss measurements; however, no differences were noted between *SR-BI*$^{-/-}$ (12.5±0.9 g/(m$^2$h)) and WT (12.5±0.7 g/(m$^2$h)) mice. Next, mLMMs were used as substitutes to investigate the specific impact of the altered epidermal FFA composition on the outside-inside lipid barrier function of *SR-BI*$^{-/-}$ mice. Small-angle X-ray diffraction showed that the lipids in the WT$_{LMM}$ and the *SR-BI*$^{-/-}_{LMM}$ were organized in both short and long periodicity phases (Figure 7a).

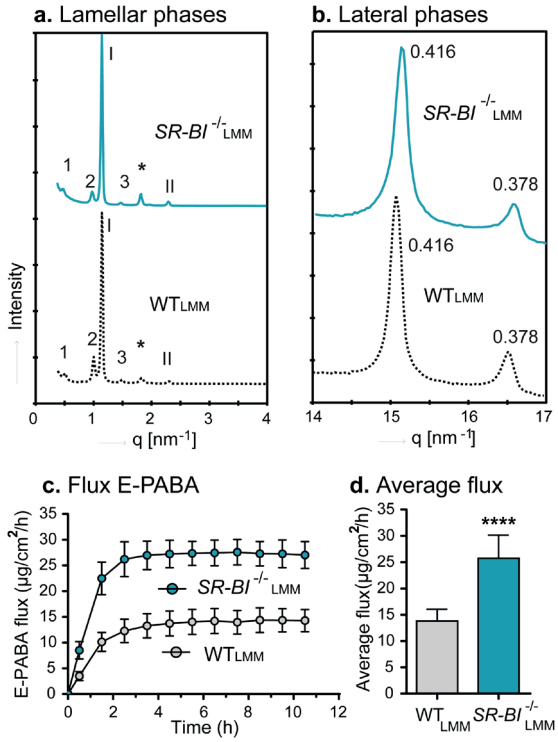


**Figure 7. Lamellar and lateral lipid organizations in the WT$_{LMM}$ and *SR-BI*$^{-/-}_{LMM}$ and their permeability to E-PABA.** a-b. Lamellar and lateral organizations of the mLMM were determined by small- and wide-angle X-ray diffraction studies, respectively. Long periodicity phase order indicated in Arabic numbers (1-3), short periodicity phase orders indicated in Roman numbers (I-II), and the reflection of crystalline cholesterol indicated with an asterisk (*). c. Permeability of WT$_{LMM}$ and *SR-BI*$^{-/-}_{LMM}$ to E-PABA over time. d. Average steady-state flux of E-PABA measured from 3.5-10.5 hours. Values are plotted as mean±SD; representative of three

different experiments (total n=6-7 mLMMs/group). Statistical significance was determined by two-tailed unpaired student's t-Test. ****$p$<0.0001.

The repeated distance of the long periodicity phase was increased in the *SR-BI*$^{-/-}_{LMM}$ compared to the $WT_{LMM}$ ($p$<0.0001), but the short periodicity phase did not differ between both mLMM (Supplementary Figure. S4). Additionally, in both $WT_{LMM}$ and the *SR-BI*$^{-/-}_{LMM}$ a high fraction of lipids in these synthetic models adopted an orthorhombic lateral packing characterized by the presence of two peaks at a position corresponding to a spacing of 0.416 nm and 0.378 nm in the wide-angle X-ray diffraction studies (Figure 7b). Next, the lipid barrier function of $WT_{LMM}$ and the *SR-BI*$^{-/-}_{LMM}$ was assessed by measuring their permeability to E-PABA. The flux of E-PABA through both types of synthetic lipid membranes reached a steady-state after 3 hours (Figure 7c). In the steady-state, the *SR-BI*$^{-/-}_{LMM}$ showed nearly 2-fold higher permeability to E-PABA compared to the control $WT_{LMM}$ (27.3±2.4 *vs*. 13.9±2.2 μg/cm$^2$/h, respectively; $p$<0.0001) (Figure 7d). At the end of the experiment, nearly 100% of E-PABA was recovered in all groups measuring the donor and acceptor phases (data not shown).

## 4. DISCUSSION

Despite the protective role of HDL in reverse cholesterol transport, we showed in this study that HDL-associated hyperalphalipoproteinemia can alter the epidermal lipid composition; thereby, negatively impacting the lipid barrier function of the skin. Additionally, these results support the hypothesis that the plasma levels of CE, independent of the type of lipoprotein carrier, play a crucial role in the maintenance of a proper skin barrier function.

Deficiency of SR-BI in mice impairs the clearance of HDL-CE from the circulation[39,40], which in turn leads to inhibition of LCAT activity and consequent FC accumulation[41]. Hence, *SR-BI*$^{-/-}$ mice, even on a low-fat/low cholesterol diet, develop a mild hyperalphalipoproteinemia characterized by increases in both FC and CE transported in the HDL fraction[10]. *In vitro*, *SR-BI* knockdown in human skin equivalents did not affect the cholesterol content of these skin models but led to downregulation of relevant lipid metabolism genes (*LDLR, PPAR-α, PPAR-γ*)[36]. Similarly, hyperalphalipoproteinemia in *SR-BI*$^{-/-}$ mice did not translate into changes in the epidermal cholesterol fraction in the skin of these mice. However, an increased flux of plasma cholesterol into their skin is expected as evidenced by downregulation of *LDLR* and *HMGCS1*; thereby, maintaining normal FC levels in the *SR-BI*$^{-/-}$ skin[11,42]. In addition, it is important to note that cholesterol

in the skin can be found as FC, CE, cholesterol sulfate and oxysterols[43,44]. In the SC, cholesterol sulfate comprises a minor fraction of the sterol content while FC is the major sterol component of the lipid matrix[45]. However, modified cholesterol species could not be measured with our LC/MS method and we cannot exclude that changes in the levels of these species contribute to the preserving the FC content in the SC.

As previously described in *APOE*$^{-/-}$ mice[11], unsaturated and short chain FFA species (below 24 carbons atoms) were strongly augmented in the epidermis of *SR-BI*$^{-/-}$ mice, which also showed downregulation of genes involved in FFA synthesis (*ACACA, FAS*) and elongation (*ELOVL1*) compared to WT controls. Although CERs and FFAs share biosynthetic pathways[46,47], the shift towards short chain and unsaturated FFA species in the *SR-BI*$^{-/-}$ epidermis did not result in a comparable profile in the CER composition, where only minor differences were observed in the percentage of a few subclasses compared to the WT controls. Thus, the altered FFA profile in the epidermal barrier of *SR-BI*$^{-/-}$ mice is likely not related to the biosynthetic pathway shared with CER but has rather an extracutaneous origin.

Analysis of the epidermal lipids also revealed increased amounts of FFA C18:1 in *SR-BI*$^{-/-}$ mice. As previously indicated, the LCAT activity is inhibited in the *SR-BI*$^{-/-}$ mice due to higher plasma levels of CE. Subbaiah *et. al.* (2013) demonstrated that low activity of LCAT in mice increases circulating levels of C16:0- and C18:1-containing CE, suggesting a direct link between C18:1-containing CE in plasma and elevated epidermal FFA C18:1[48]. The changes in the epidermal FFA species of the mild hypercholesterolemic *SR-BI*$^{-/-}$ mice showed a similar trend as that recently reported for the severely hypercholesterolemic *APOE*$^{-/-}$ mice[11]. In addition to their increased circulating CE concentrations, the epidermis of both *SR-BI*$^{-/-}$ and *APOE*$^{-/-}$ mice are enriched in FFA C18:1 and FFA C20:1, though to a lesser extend in the epidermis of *SR-BI*$^{-/-}$ mice. Simultaneous exposure of HaCaT keratinocytes to FFA C18:1 and 25-hydroxy cholesterol resulted in downregulation of HMGCoA synthase and a lower rate of acetate incorporation into FFA synthesis[42]. Hence, a higher flux of plasma CE into the epidermis of *SR-BI*$^{-/-}$ mice (similar to *APOE*$^{-/-}$mice) can be expected, which is also supported by the strong correlations between plasma CE and epidermal FFA C18:1 and the robust correlation between epidermal C18:1 and its elongated product FFA C20:1 in the epidermis.

Alterations in the epidermal lipid composition can affect the lipid organization and the functionality of the skin barrier[47]. In particular, short and unsaturated FFAs have been described to reduce the density of the lipid packing even in the presence of a similar CER composition[49,50]. Here, we analyzed the contribution of the altered lipid profile to the outside-inside lipid barrier function using LMMs. Our results show that a minor

increase in the short chain FFA fraction in LMMs can preserve the dense orthorhombic packing while increasing the mobility of the lipids within the lipid matrix, which in turn translates into a more permeable outside-inside lipid barrier[51]. In vivo transepidermal water loss measurements in *SR-BI*$^{-/-}$ mice revealed a functional inside-outside skin barrier despite the alteration in epidermal lipids (enriched in short chain FFAs). It is important to note that in the in vivo situation trans-corneocytes water transport, as well as hair follicles and other surface lipids will contribute to/influence the maintenance of transepidermal water loss levels. Hence, although the barrier lipids in the *SR-BI*$^{-/-}$ epidermis showed a dense orthorhombic organization, the lipid composition of the *SR-BI*$^{-/-}_{LMM}$ (enriched in short chain FFAs) resulted in a more permeable outside-inside lipid barrier.

Although SR-BI is expressed in both murine and human keratinocytes, its specific contribution to the skin lipid homeostasis is not yet clear due the lack of an *in vivo* keratinocyte-specific knockout mouse model. Recent data from a study using *SR-BI* knockout human skin equivalents suggests an involvement of SR-BI in lipid regulation in the upper epidermal layer; in particular in CER metabolism[36]. In our study, the CER composition was preserved in the total body *SR-BI*$^{-/-}$ mice while both cholesterol and FFA metabolism were shifted to a compensatory gene expression profile. This indicates that the hyperalphalipoproteinemia rather than the local absence of SR-BI in the skin may be the driving factor to the observed changes in epidermal lipids in these mice.

In conclusion, this study shows that hypercholesterolemia-related to elevated circulating levels of HDL particles alters the epidermal lipid composition, resulting in a compromised lipid barrier function in young adult *SR-BI*$^{-/-}$ mice on a low fat chow diet. In addition, a clear correlation between plasma CE levels and epidermal levels of FA C18:1 and FA C20:1 in hypercholesterolemic mice indicates that increased circulating CE may have a decisive role in the development of this skin phenotype. Although to date skin related problems have not been described in patients with SR-BI polymorphisms or hyperalphalipoproteinemia, this study demonstrates the relevance of analyzing the SC lipid composition in these patients to prevent the development of upcoming abnormalities in the functionality of the skin barrier.

**CONFLICT OF INTEREST**

The authors have no conflict of interest to declare regarding the content of this research article.

**ACKNOWLEDGEMENTS**

We thank the support of the DUBBLE beam line personnel in performing the X-ray diffraction studies at the European Synchrotron Radiation Facility (Grenoble, France), and the company Evonik (Essen, Germany) for providing us the synthetic ceramides used in our LC/MS analysis and in the preparation of our LMMs. We also thank Walter Boiten and Andreea Nădăban for their assistance with the interpretation of the MS/MS fragmentation data and Miréia N. A. Bernabé Kleijn for her assistance with transepidermal water loss measurements. This research was funded by the Leiden Academic Centre for Drug Research (Leiden, The Netherlands).

## REFERENCES

1. Elias, P. M. Stratum corneum defensive functions: An integrated view. J. Invest. Dermatol. 125, 183–200 (2005).

2. Ponec, M., Weerheim, A., Lankhorst, P. & Wertz, P. New acylceramide in native and reconstructed epidermis. J. Invest. Dermatol. 120, 581–588 (2003).

3. Rassner, U., Feingold, K. R., Crumrine, D. A. & Elias, P. M. Coordinate assembly of lipids and enzyme proteins into epidermal lamellar bodies. Tissue Cell 31, 489–498 (1999).

4. Tsuruoka, H. et al. Scavenger receptor class B type I is expressed in cultured keratinocytes and epidermis. Regulation in response to changes in cholesterol homeostasis and barrier requirements. J. Biol. Chem. 277, 2916–2922 (2002).

5. Khnykin, D., Miner, J. H. & Jahnsen, F. Role of fatty acid transporters in epidermis. Dermatoendocrinol. 3, 53–61 (2011).

6. Haruta-Ono, Y. et al. Orally administered sphingomyelin in bovine milk is incorporated into skin sphingolipids and is involved in the water-holding capacity of hairless mice. J. Dermatol. Sci. 68, 56–62 (2012).

7. Abd El-Latif, M. I. A., Murota, H., Terao, M. & Katayama, I. Effects of a 3-hydroxy-3-methylglutaryl coenzyme A reductase inhibitor and low-density lipoprotein on proliferation and migration of keratinocytes. Br. J. Dermatol. 128–137 (2010). doi:10.1111/j.1365-2133.2010.09694.x

8. Accad, M. et al. Massive xanthomatosis and altered composition of atherosclerotic lesions in hyperlipidemic mice lacking acyl CoA:cholesterol acyltransferase 1. J. Clin. Invest. 105, 711–719 (2000).

9. Ishibashi, S., Goldstein, J. L., Brown, M. S., Herz, J. & Burns, D. K. Hypercholesterolemia in low density lipoprotein receptor knockout mice and its reversal by adenovirus-mediated gene delivery. J. Clin. Invest. 92, 883–93 (1993).

10. Van Eck, M. et al. Differential effects of scavenger receptor BI deficiency on lipid metabolism in cells of the arterial wall and in the liver. J. Biol. Chem. 278, 23699–23705 (2003).

11. Martins Cardoso, R. et al. Hypercholesterolemia in young adult APOE −/− mice alters epidermal lipid composition and impairs barrier function. Biochim. Biophys. Acta - Mol. Cell Biol. Lipids 1864, 976–984 (2019).

12. Vaughan, A. M. & Oram, J. F. ABCA1 and ABCG1 or ABCG4 act sequentially to remove cellular cholesterol and generate cholesterol-rich HDL. J. Lipid Res. 47, 2433–2443 (2006).

13. Nakamura, Y. et al. Molecular Mechanism of Reverse Cholesterol Transport: Reaction of Pre-β-Migrating High-Density Lipoprotein with Plasma Lecithin/Cholesterol Acyltransferase †. Biochemistry 43, 14811–14820 (2004).

14. Acton, S. et al. Identification of Scavenger Receptor SR-BI as a High Density Lipoprotein Receptor. Science (80-. ). 271, 518–520 (1996).

15. Out, R. et al. Scavenger receptor class B type I is solely responsible for the selective uptake of cholesteryl esters from HDL by the liver and the adrenals in mice. J. Lipid Res. 45, 2088–2095 (2004).

16. Krieger, M. Scavenger receptor class b type I is a multiligand hdl receptor that influences diverse physiologic systems. J. Clin. Invest. 108, 793–797 (2001).

17. Shen, W.-J., Asthana, S., Kraemer, F. B. & Azhar, S. Scavenger receptor B type 1: expression, molecular regulation, and cholesterol transport function. J. Lipid Res. 59, 1114–1131 (2018).

18. Lin, M.-H. & Khnykin, D. Fatty acid transporters in skin development, function and disease. Biochim. Biophys. Acta 1841, 362–8 (2014).

19. Mommaas, M., Tada, J. & Ponec, M. Distribution of low-density lipoprotein receptors and apolipoprotein B on normal and on reconstructed human epidermis. J. Dermatol. Sci. 2, 97–105 (1991).

20. Randolph, G. J., Miller, N. E., Randolph, G. J. & Miller, N. E. Lymphatic transport of high-density lipoproteins and chylomicrons Find the latest version : Review series Lymphatic transport of high-density lipoproteins and chylomicrons. 124, 929–935 (2014).

21. Huang, L. et al. Interleukin-17 Drives Interstitial Entrapment of Tissue Lipoproteins in Experimental Psoriasis. Cell Metab. 29, 475-487.e7 (2019).

22. Brunham, L. R. et al. Novel mutations in scavenger receptor BI associated with high HDL cholesterol in humans. Clin. Genet. 79, 575–581 (2011).

23. Vergeer, M. et al. Genetic Variant of the Scavenger Receptor BI in Humans. N. Engl. J. Med. 364, 136–145 (2011).

24. Korporaal, S. J. A. et al. Deletion of the High-Density Lipoprotein Receptor Scavenger Receptor BI

in Mice Modulates Thrombosis Susceptibility and Indirectly Affects Platelet Function by Elevation of Plasma Free Cholesterol. Arterioscler. Thromb. Vasc. Biol. 31, 34–42 (2011).

25. Dole, V. S. et al. Thrombocytopenia and Platelet Abnormalities in High-Density Lipoprotein Receptor–Deficient Mice. Arterioscler. Thromb. Vasc. Biol. 28, 1111–1116 (2008).

26. Cai, L., Ji, A., de Beer, F. C., Tannock, L. R. & van der Westhuyzen, D. R. SR-BI protects against endotoxemia in mice through its roles in glucocorticoid production and hepatic clearance. J. Clin. Invest. 118, 364–375 (2008).

27. Hoekstra, M. et al. Absence of HDL cholesteryl ester uptake in mice via SR-BI impairs an adequate adrenal glucocorticoid-mediated stress response to fasting. J. Lipid Res. 49, 738–745 (2008).

28. Out, R. et al. Macrophage ABCG1 Deletion Disrupts Lipid Homeostasis in Alveolar Macrophages and Moderately Influences Atherosclerotic Lesion Development in LDL Receptor-Deficient Mice. Arterioscler. Thromb. Vasc. Biol. 26, 2295–2300 (2006).

29. Boiten, W., Absalah, S., Vreeken, R., Bouwstra, J. & van Smeden, J. Quantitative analysis of ceramides using a novel lipidomics approach with three dimensional response modelling. Biochim. Biophys. Acta - Mol. Cell Biol. Lipids 1861, 1652–1661 (2016).

30. Motta, S. et al. Ceramide composition of the psoriatic scale. BBA - Mol. Basis Dis. 1182, 147–151 (1993).

31. Smith, K. R. & Thiboutot, D. M. Thematic review series: Skin Lipids. Sebaceous gland lipids: friend or foe? J. Lipid Res. 49, 271–281 (2008).

32. Westerberg, R. et al. Role for ELOVL3 and Fatty Acid Chain Length in Development of Hair and Skin Function. J. Biol. Chem. 279, 5621–5629 (2004).

33. Chomczynski, P. & Sacchi, N. The single-step method of RNA isolation by acid guanidinium thiocyanate–phenol–chloroform extraction: twenty-something years on. Nat. Protoc. 1, 581–585 (2006).

34. van Smeden, J. et al. LC/MS analysis of stratum corneum lipids: ceramide profiling and discovery. J. Lipid Res. 52, 1211–1221 (2011).

35. Ohno, Y. et al. ELOVL1 production of C24 acyl-CoAs is linked to C24 sphingolipid synthesis. Proc. Natl. Acad. Sci. 107, 18439–18444 (2010).

36. Muresan, X. M. et al. Involvement of cutaneous SR-B1 in skin lipid homeostasis. Arch. Biochem. Biophys. 666, 1–7 (2019).

37. Mohd, F., Todo, H., Yoshimoto, M., Yusuf, E. & Sugibayashi, K. Contribution of the hair follicular pathway to total skin permeation of topically applied and exposed chemicals. Pharmaceutics 8, (2016).

38. Blume-Peytavi, U. et al. Follicular and percutaneous penetration pathways of topically applied minoxidil foam. Eur. J. Pharm. Biopharm. 76, 450–453 (2010).

39. Brodeur, M. R., Luangrath, V., Bourret, G., Falstrault, L. & Brissette, L. Physiological importance of SR-BI in the in vivo metabolism of human HDL and LDL in male and female mice. J. Lipid Res. 46, 687–696 (2005).

40. Rigotti, A. et al. A targeted mutation in the murine gene encoding the high density lipoprotein (HDL) receptor scavenger receptor class B type I reveals its key role in HDL metabolism. Proc. Natl. Acad. Sci. U. S. A. 94, 12610–12615 (1997).

41. Kosek, A. B., Durbin, D. & Jonas, A. Binding affinity and reactivity of lecithin cholesterol acyltransferase with native lipoproteins. Biochem. Biophys. Res. Commun. 258, 548–551 (1999).

42. Siefken, W., Höppner, H. & Harris, I. R. Regulation of cholesterol synthesis by oleic and palmitic acid in keratinocytes. Exp. Dermatol. 9, 138–145 (2000).

43. Sjövall, P. et al. Imaging the distribution of skin lipids and topically applied compounds in human skin using mass spectrometry. Sci. Rep. 8, 1–14 (2018).

44. Feingold, K. R. & Jiang, Y. J. The mechanisms by which lipids coordinately regulate the formation of the protein and lipid domains of the stratum corneum: Role of fatty acids, oxysterols, cholesterol sulfate and ceramides as signaling molecules. Dermatoendocrinol. 3, 113–118 (2011).

45. Elias, P. M., Williams, M. L., Choi, E. H. & Feingold, K. R. Role of cholesterol sulfate in epidermal structure and function: Lessons from X-linked ichthyosis. Biochim. Biophys. Acta - Mol. Cell Biol. Lipids 1841, 353–361 (2014).

46. Sassa, T. et al. Impaired Epidermal Permeability Barrier in Mice Lacking Elovl1, the Gene Responsible for Very-Long-Chain Fatty Acid Production. Mol. Cell. Biol. 33, 2787–2796 (2013).

47. van Smeden, J. et al. The importance of free fatty acid chain length for the skin barrier function in atopic eczema patients. Exp. Dermatol. 23, 45–52 (2014).

48. Subbaiah, P. V. et al. Regulation of plasma cholesterol esterification by sphingomyelin: Effect of physiological variations of plasma sphingomyelin on lecithin-cholesterol acyltransferase activity. Biochim. Biophys. Acta - Mol. Cell Biol. Lipids 1821, 908–913 (2012).

49. Mojumdar, E. H., Helder, R. W. J., Gooris, G. S. & Bouwstra, J. A. Monounsaturated fatty acids reduce the barrier of stratum corneum lipid membranes by enhancing the formation of a hexagonal lateral packing. Langmuir 30, 6534–6543 (2014).

50. Groen, D., Poole, D. S., Gooris, G. S. & Bouwstra, J. A. Is an orthorhombic lateral packing and a proper lamellar organization important for the skin barrier function? Biochim. Biophys. Acta - Biomembr. 1808, 1529–1537 (2011).

51. Uchiyama, M., Oguri, M., Mojumdar, E. H., Gooris, G. S. & Bouwstra, J. A. Free fatty acids chain length distribution affects the permeability of skin lipid model membranes. Biochim. Biophys. Acta - Biomembr. 1858, 2050–2059 (2016).

## SUPPLEMENTARY INFORMATION

# 1. METHODS

## 1.1 Liquid chromatography-mass spectrometry (LC/MS)

**Table S1. Gradient of solvents used for cholesterol and CER analysis by UPLC-LC/MS.**

| Run time (min) | Solvent A[1] (%) | Solvent B[2] (%) |
|---|---|---|
| 0 | 98 | 2 |
| 2.5 | 96 | 4 |
| 2.6 | 93 | 7 |
| 6 | 88 | 12 |
| 11 | 50 | 50 |
| 13 | 98 | 2 |

**[1]Solvent A - 100% Heptane**

**[2]Solvent B -Heptane:isopropanol:ethanol - 50:25:25; v/v/v**

**Table S2. Gradient of the solvents used for FFA analysis by UPLC-LC/MS.**

| Run time (min) | Solvent A[1] (%) | Solvent B[2] (%) |
|---|---|---|
| 0 | 100 | 0 |
| 2.5 | 0 | 100 |
| 5 | 0 | 100 |
| 8 | 100 | 0 |
| 11 | 100 | 0 |

**[1]Solvent A - Acetonitrile/milliQ/chloroform/acetic acid -90:10:2:0.005; v/v/v/v**

**[2]Solvent B -Methanol/heptane/chloroform/acetic acid -90:10:2:0.005; v/v/v/v**

## 1.3. Quantitative real-time PCR (q-PCR)

**Table S3. Forward and reverse primer sequences used for q-PCR.**

| Protein (Gene) | Forward primer Reverse primer |
|---|---|
| Ribosomal protein, large, P0 (RPL0) | CTGAGTACACCTTCCCACTTACTGA CGACTCTTCCTTTGCTTCAGCTTT |
| Cytochrome c-1 (CYC1) | ACTGGGGTGTCATTGCGAGAAGGC GGTCATGCTCTGGTTCTGATGCCCA |
| Ribosomal protein S20 (RPS20) | GGACTTGATCAGAGGCGCCAAGGAAA CCCAGGTCTTGGAACCTTCACCACAA |
| Acetyl-Coenzyme A carboxylase alpha (ACACA) | GGAAGATGGCGTCCGCTCTGTG GTGAGATGTGCTGGGTCATGTGGAC |
| ATP-binding cassette, subfamily A, member 1 (ABCA1) | AGAGCAAAAAGCGACTCCACATAGAA CGGCCACATCCACAACTGTCT |
| ATP-binding cassette, subfamily A, member 12 (ABCA12) | TGACCTTCTGGAAACCAACAAGACTGC CACTTATGGTGGAACCTTGGCTACTGG |
| ATP-binding cassette, subfamily G, member 1 (ABCG1) | TTGACACCATCCCAGCCTAC CAGTGCAGGTCTTCTCGGT |
| Aldehyde dehydrogenase family 3, subfamily A2 (ALDH3A2) | CGGGTGATAGATGAGACCTCCAGTGG AGGGGCGCTGATGAGAAAAGGTATCA |
| N-acylsphingosine amidohydrolase 1 (ASAH1) | TTATTGATGACCGCAGAACACCGGC TACAAGGGTCTGGGCAATCTCGAAGG |
| Ceramide kinase 1 (CERK1) | CTTGCTCAGCCTCCAGAAGCTCCT TCCTGGGCTTTGGGGTTCTTGCTTA |
| Ceramide synthase 3 (CERS3) | GGGCCTCCACGTTTACTGGGGT GCCCTTGGTGCTCTCTGCTTCCT |
| Elongation of very long chain fatty acids 1 (ELOVL1) | GGCAGAACTTGCCCCTGAGAAGAA TTCACAACAGCCTCCATCCTGGC |
| Elongation of very long chain fatty acids 4 (ELOVL4) | TGGAATCAAGTGGGTGGCTGGAGG AGCATGGTCAGGTATCGCTTCCACC |
| Elongation of very long chain fatty acids 6 (ELOVL6) | GGACCTGTCAGCAAATTCTGGGCTTA GGAGTACCAGGAGTACAGGAGCACA |
| Elongation of very long chain fatty acids 7 (ELOVL7) | ACAGCTGTGCACGTGGTCATGTATTC ACTGGGTACTGGTAATTGCAGTCCTCC |
| Fatty acid synthase (FAS) | GGCGGCACCTATGGCGAGG CTCCAGCAGTGTGCGGTGGTC |
| Glucocerebrosidase (GBA) | GCCCTTGCCAACAGTTCCCATGATG TGCCATGAACGTACTTAGCTGCCTCT |
| 2-hydroxyacyl-CoA lyase 1 (HACL1) | GGTTTTGACGCTGACACCTGGGAAA CCTCAGCGAGTGTTGGAGCTCTTCT |
| 3-hydroxy-3-methylglutaryl-CoA synthase 1 (HMGCS1) | AAAACACAGAAGGACTTACGCCCGG GTTGCAGGGAGTCTTGGCACTTTCT |
| Low density lipoprotein receptor (LDLR) | TGTGTGATGGAGACCGAGATTG CGTCAACACAGTCGACATCC |

| Protein (Gene) | Forward primer Reverse primer |
|---|---|
| Stearoyl-Coenzyme A desaturase 1 (SCD1) | TACTACAAGCCCGGCCTCC CAGCAGTACCAGGGCACCA |

## 2. RESULTS



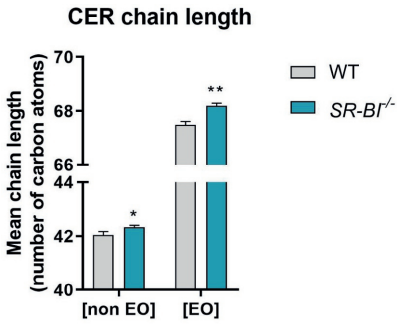


**Figure S1. CER average chain length.** Average total chain length of CERs with non-ω-esterified (CER[nonEO]) and ω-esterified (CER[EO]) fatty acid chains in their acyl chain. Values are plotted as mean ±SD (n=3 animals/group). Statistical significance was determined by unpaired students t-Test. *$p$<0.05, **$p$<0.01.

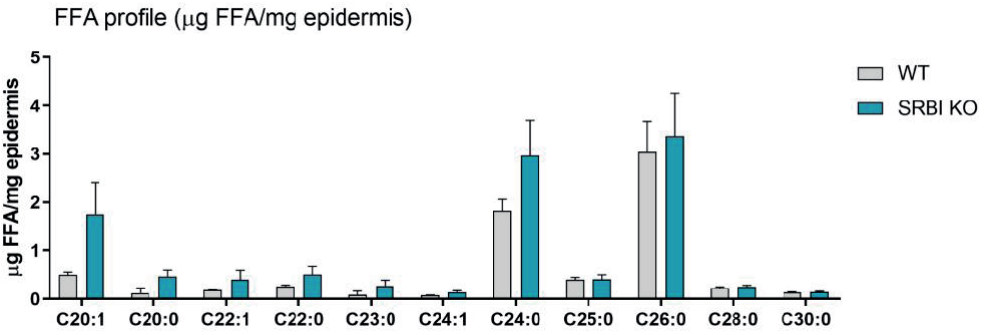


**Figure S2. FFA composition in absolute values. FFA composition was determined by LC/MS.** Values are plotted as mean ±SD (n=3 animals/group).

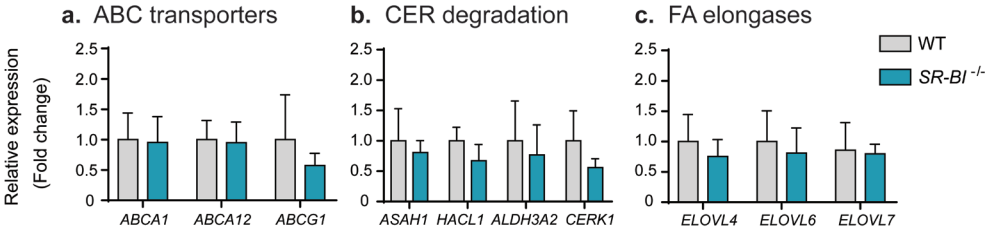


**Figure S3. Expression of genes involved in lipid synthesis in the skin.** Relative mRNA levels of (a) ABC transporters, (b) CER degradation enzymes, and (c) FA elongases. Genes and their respective encoded proteins/receptors: ABCA1 – ATP-binding cassette, subfamily A, member 1; ABCA12 – ATP-binding cassette, subfamily A, member 12; ABCG1 – ATP-binding cassette, subfamily G, member 1; ASAH1– N-acylsphingosine amidohydrolase 1; HACL1 – 2-hydroxyacyl-CoA lyase 1; ALDH3A2 – Aldehyde dehydrogenase family 3, subfamily A2; CERK1 – Ceramide kinase 1; ELOVL4 - elongase of very long chain fatty acids 4; ELOVL6 - elongase of very long chain fatty acids 6; ELOVL7 - elongase of very long chain fatty acids 7. Values are plotted as mean±SD and represent the fold change expression compared to the WT control (n=5-6 animals/group).

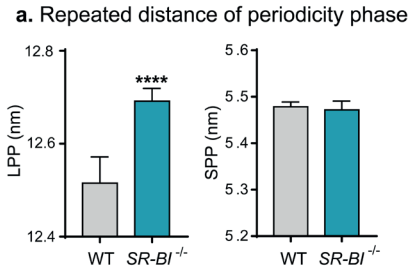


**Figure S4. Repeated distances of the lamellar phases in WT and *SR-BI*$^{-/-}_{LMM}$.** Repeated distances in the logng and short periodicity phases were determined by small-angle X-ray diffraction studies. espectively. Values are plotted as mean±SD (n=3 mLMM/group). Statistical significance was determined by unpaired students t-Test. ****$p$<0.000